Supplementary Information

for

$MgAl_2O_4$ nanoparticles: A new low-density additive for accelerated thermal decomposition of ammonium perchlorate

Xiangfeng Guan,[1] Liping Li,[2] Jing Zheng[2], and Guangshe Li,[1,*]

[1] State Key Laboratory of Structural Chemistry, Fujian Institute of Research on the Structure of Matter, Chinese Academy of Sciences, Fuzhou 350002, P. R. China

[2] Key Laboratory of Optoelectronic Materials Chemistry and Physics, Chinese Academy of Sciences, Fuzhou 350002, P. R. China

* Corresponding author: Prof. G.S. Li, E-mail: guangshe@ fjirsm.ac.cn.

Tel./Fax: (+86) 591-83702122

S1:

Figure S1 The results of elemental mapping of sample S-600, S-800, and S-900 by EDS

A: SEM image (a), elemental mapping of the Mg (b) and Al (c) content, and EDS spectrum (d) of sample S-600.

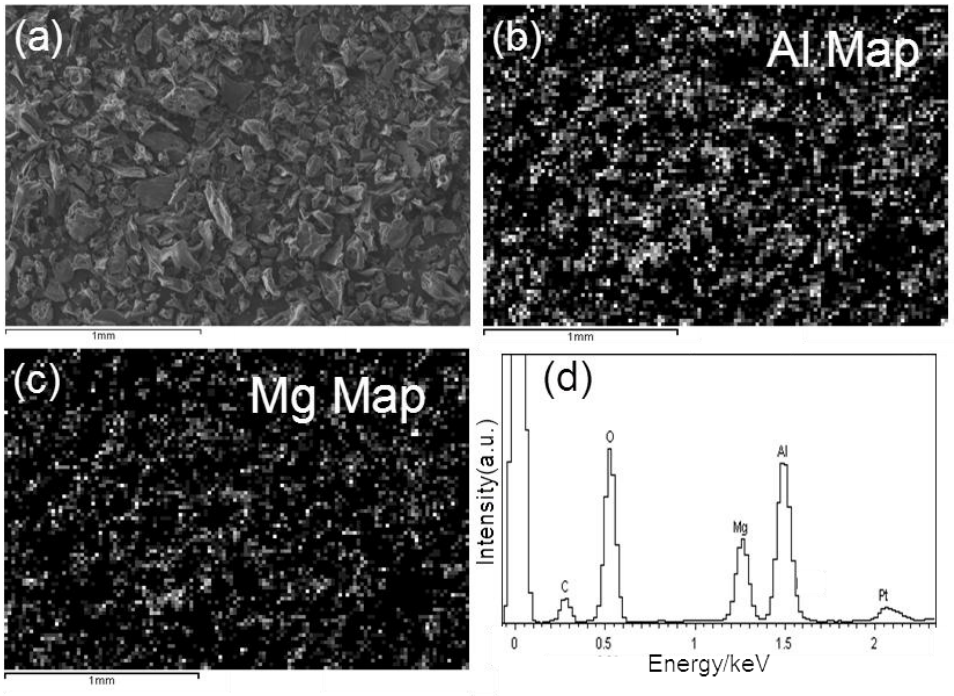

B: SEM image (a), elemental mapping of the Mg (b) and Al (c) content, and EDS spectrum (d) of sample S-800.

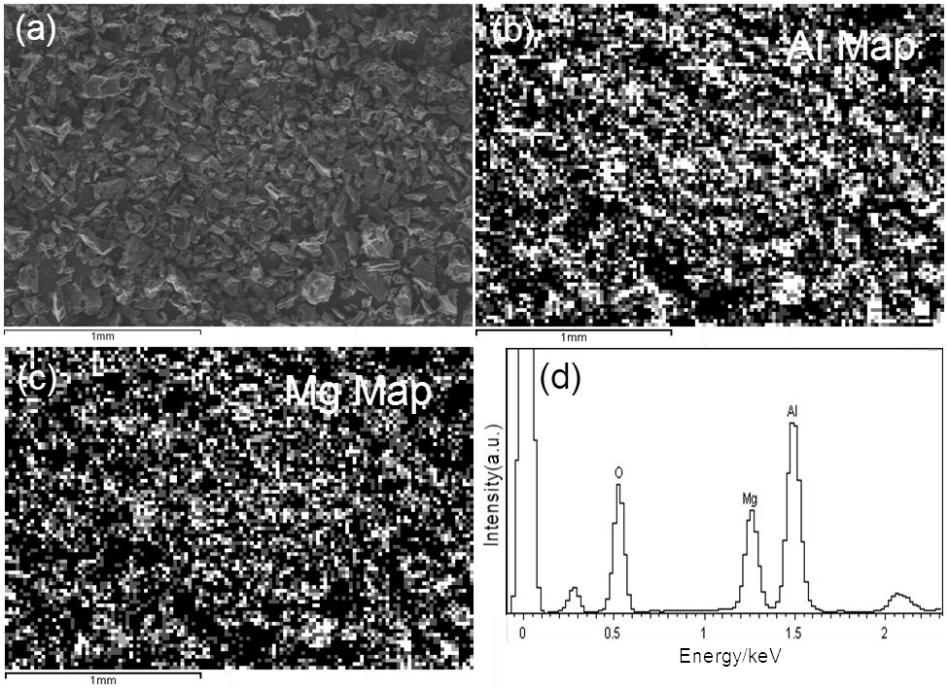

C: SEM image (a), elemental mapping of the Mg (b) and Al (c) content, and EDS spectrum (d) of sample S-900.

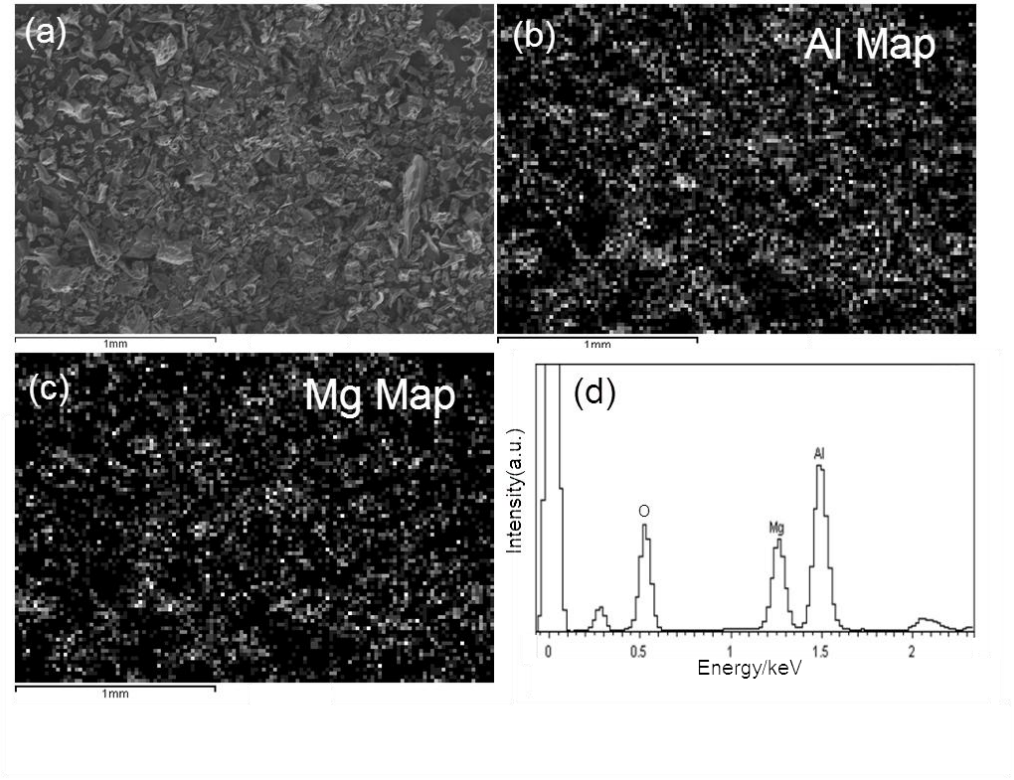

Figure S1 shows the elemental mapping of sample S-600, S-800, and S-900 by EDS. The results showed that the Mg and Al elements are homogeneously distributed in all samples and no severe heterogeneity in Mg or Al distribution was observed, further confirming the single-phase character of the annealed samples.

S2:

Figure S2 BJH desorption size distribution of the samples.

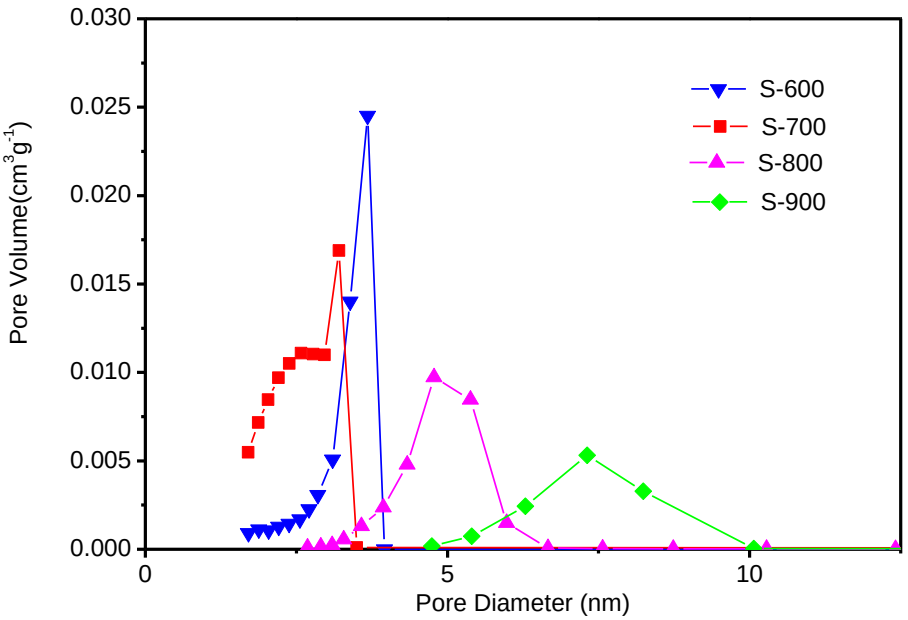

Figure S2 shows the BJH desorption pore size distribution of the samples. As can be seen, compared with BJH adsorption pore size distribution (figure 4(b)), the pore size distribution for all samples become narrower and the maximum pore diameters for sample S-700 and S-800 were apparently changed. The maximum pore diameter for sample S-700 was increased from 2.6 nm to 3.2 nm, while that for sample S-800 was decreased from 6.7 nm to 4.7 nm.

S3:

Figure S3 TEM images of as-prepared samples: (a) S-P; (b) S-600; (c) S-700; (d) S-800; (e) S-900. The insets show the corresponding selected area electron diffraction pattern (SAED).

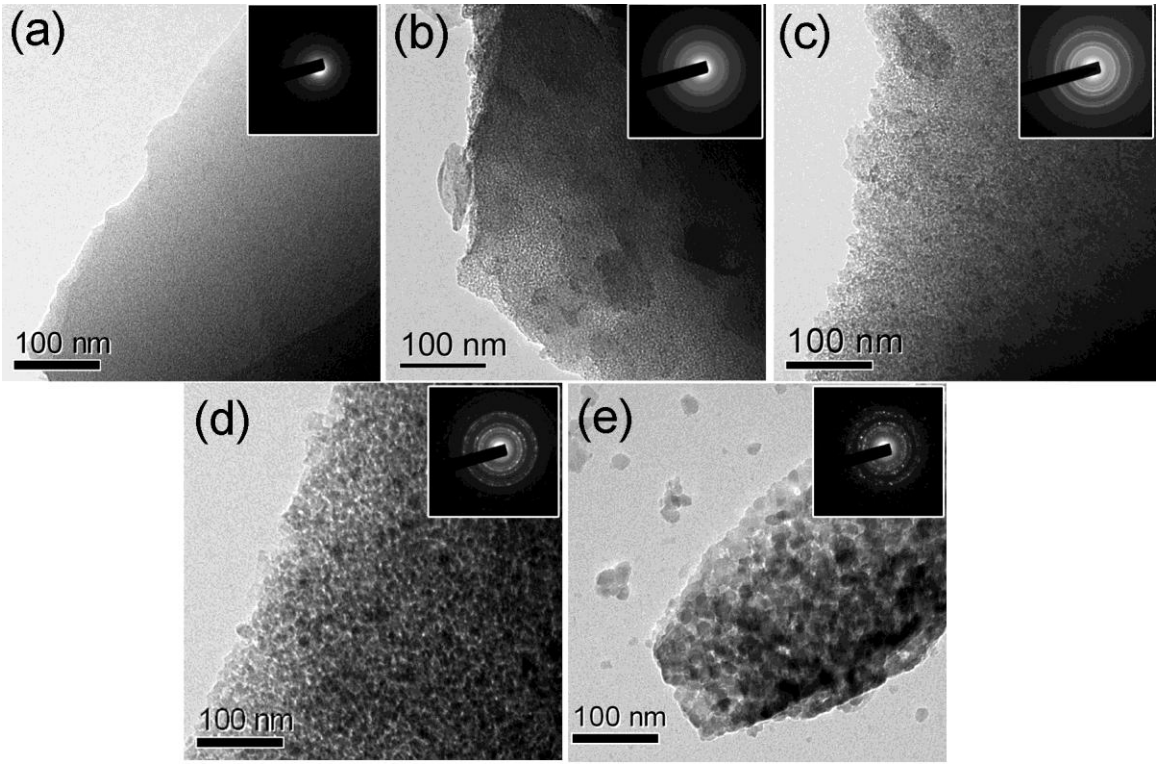

Figure S3 gives the TEM images of the samples. For sample S-P, many nanoparticles with unclear lattice fringes are dispersed homogeneously in an amorphous sheet-like matrix, which is due to the uniform distribution of metal cations on an atomic level under the chelating effect of citric acid. The corresponding SAED patterns (inset of figure S3(a)) also show the almost completely amorphous character, which indicates that self-generated amorphous carbon template was tightly around poor crystallized $MgAl_2O_4$ and can serve as the growth inhibitor of nanoparticles. After annealing in air, all the samples are composed of small crystallized $MgAl_2O_4$

nanoparticles, and these nanoparticles are cross-linked with each other to form porous structure (figure S3(b)-(e)). It indicates that the self-generated carbon template can be effectively removed by annealing in air. With the increase of annealing temperature up to 900 ^{o}C, the porous structure still retained, showing the high stability of porous structure produced by self-generated carbon template. The selected area electron diffraction (SAED) patterns indicate an increase in crystallinity with annealing temperature.

S4:

Figure S4. FTIR spectra of the samples: (a) S-600; (b) S-700; (c) S-800; and (d) S-900.

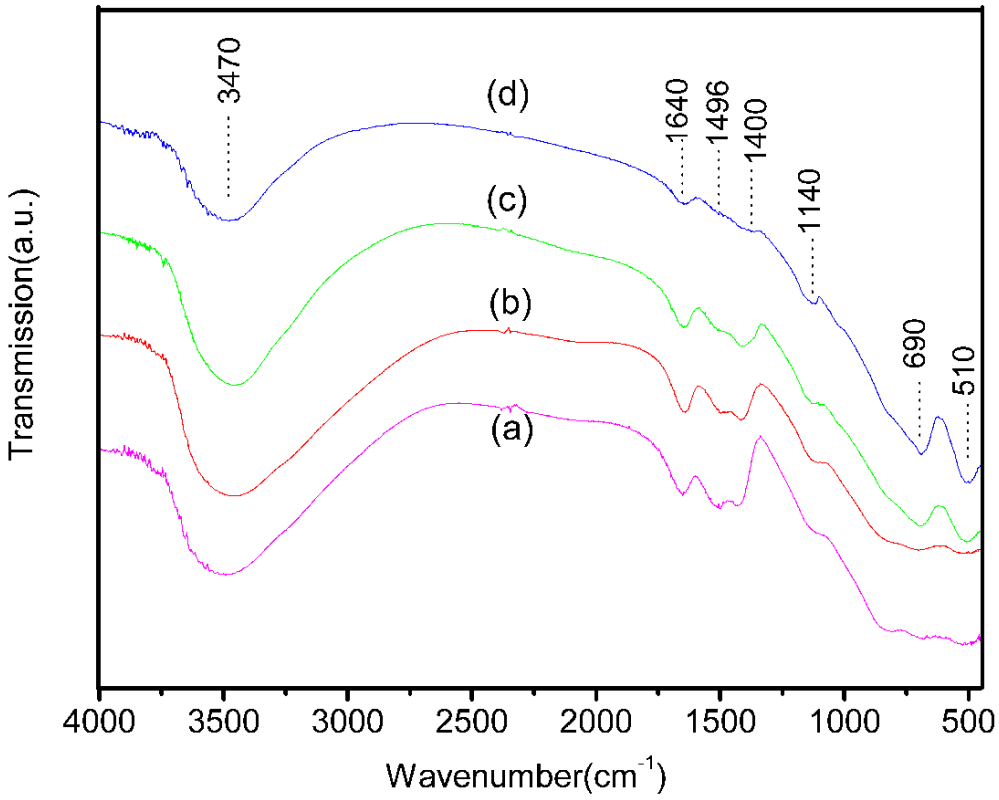

As indicated in figure S4, all samples showed similar infrared spectra. A set of bands observed in the range from 1500 to 1120 cm^{-1} are associated with the carbonate species. It is well known that $MgAl_2O_4$ crystallizes in a spinel structure, and therefore the normal lattice vibrations at Γ point of the Brillouin zone can be represented by $\Gamma(k=0)= 1A_{1g} + 1E_g + 3T_{2g} + 4T_{1u} + T_{1g} + 2A_{2u} + 2E_u + 2T_{2u}$. Among these 16 optical phonons, A_{1g} , E_g and T_{2g} are Raman active and the total number is five, while four T_{1u} are IR active modes [1]. For the as-prepared samples, the bands observed at 690 and 510 cm^{-1} are assigned to the IR active T_{1u} mode of Al-O stretching vibration. With increasing the annealing temperature, the bands at 690 and 510 cm^{-1} gradually became sharper. Since these bands correspond to the AlO_6 groups that built up the $MgAl_2O_4$ spinel [2], it indicates the formation of $MgAl_2O_4$ spinel for all the samples. The OH^- bonding characteristics of the water molecules associated with the surface hydration layer were observed. Since the signals of CO_2 and H_2O in air have already been subtracted, the FTIR data in figure S4 represent the characteristic absorbance of the samples. The water absorbed on $MgAl_2O_4$ surfaces was also confirmed by the vibrations of OH bonds as featured by the broad band centered around 3470 cm^{-1} as well as the deformation vibration for H-O-H bonds of the physisorbed water band centered around 1640 cm^{-1} [3, 4]. It should be noted that the intensities of these bands did not weaken drastically even when the annealing temperature was increased up to 900 ^oC (sample S-900), which could be probably ascribed to the porous nature of the samples.

References

[1] Ishii M, Hiraishi J and Yamanaka T 1982 Structure and lattice vibrations of Mg-Al spinel solid solution. *Phys. Chem. Mineral* **8** 64-68

[2] McMillan P and Pirious B 1982 The structure and vibrational spectra of crystals and glasses in the silica-alumina system. *J Non-Cryst. Solids* **53** 279-298

[3] White W B and De Angelis B A 1967 Interpretation of the vibrational spectra of spinels *Spectrochim. Acta* **23A** 985–995

[4] Duan X L, Song C F, Wu Y C, Yu F P, Cheng X F and Yuan D R 2008 Preparation and optical properties of nanoscale $MgAl_2O_4$ powders doped with Co^{2+} ions *J. Non-Cryst. Solids* **354** 3516-3519